

Double layered plasmonic thin-film luminescent solar concentrators based on polycarbonate supports



S.M. El-Bashir^{a,b,*}, F.M. Barakat^a, M.S. AlSalhi^a

^a Department of Physics & Astronomy, Science College, King Saud University, Riyadh, Saudi Arabia

^b Department of Physics, Faculty of Science, Benha University, Egypt

ARTICLE INFO

Article history:

Received 9 December 2012

Accepted 8 October 2013

Available online

Keywords:

Plasmonic luminescent solar concentrators

Nanogold

Photostability

Light harvesting

Power conversion efficiency

Silicon solar cells

ABSTRACT

Plasmonic thin-film luminescent solar concentrators (PTLSCs) were prepared by coating polycarbonate substrates with fluorescent PMMA films doped with coumarin dyes, nanogold and nanosilver molecules. The study of the absorption and fluorescence spectra showed a highly efficient light harvesting accompanied with metal enhanced fluorescence (MEF) of PTLSC films. The photostability measurements showed a decrease of the dye photodegradation rates by increasing nanogold concentration. The indoor testing of PTLSCs showed that the enhancement of the output power conversion efficiency was 53.2%, 33.4% and 25.8% obtained for a-Si and mc-Si and c-Si PV cells respectively. The field performance of PTLSCs under diffused radiation was evaluated by outdoor testing in Riyadh city (KSA) during winter and spring seasons, the study revealed that the maximum solar electrical conversion is well correlated to the solar irradiance type at the location.

© 2013 Elsevier Ltd. All rights reserved.

1. Introduction

Solar energy has long been publicized as better for the environment than fossil fuels since it reduces hazardous greenhouse gases such as CO₂ which affects the earth's temperature [1]. Silicon photovoltaic (PV) cells, solar-thermal-heating and concentrating systems are some examples of promising candidates of solar technology applications [2]. Among these examples thin film luminescent solar concentrators (TLSCs) are currently experiencing substantial investment and growth, driven by the aim of generating low cost solar electricity. One approach is to reduce the amount of semiconductor material utilized, which is facilitated by concentrating the solar power from a large aperture area to a smaller area using inexpensive concentration techniques [3,4]. The basic idea of TLSC is based on the absorption of incident sunlight by a luminescent film coated on a transparent plate with a high refractive index, then the luminescence is emitted with high quantum efficiency and finally be collected and guided by total internal reflection to the plate edge where small area PV cells are attached [5]. The marketable applications of TLSCs have been hindered by three major problems; many of fluorescent materials have poor

absorption over the visible region of the solar spectrum, thus limiting the amount of converted solar spectra. Also, many of fluorescing materials photodegrade too quickly, limiting the lifetime of the device. Finally, the spectral overlap between the absorption and fluorescence spectra of the fluorophores causes the re-absorption losses which increase as the size of the TLSC increases [6]. As the light-harvesting area of the PV system is much smaller than that of the TLSC system, the efficiency and reducing the cost of solar cells are potentially improved [7]. TLSCs have several advantages such as reducing of self-absorption and scattering loss, utilizing full solar spectrum stacking plates which are containing different types of luminescent species, reducing the fabrication cost as less doped material required for thin film than being doped in the bulk plate [8]. Recently, more research efforts are in progress to improve cost effective employments of these concentrators such as wedge-shaped geometry [9] and flexible substrates [10]. The main disadvantage of TLSCs is that the solar radiation is absorbed by a small volume of the thin film leading to a decrease in the overall output of the device. This problem could be solved using the plasmonic properties of noble metal nanoparticles (MNPs) [11]. Metallic nanostructures have been introduced into thin inorganic semiconductor solar cells (e.g., Si, GaAs solar cells) for highly efficient light harvesting by expected light-scattering behavior and a strong near-field by the plasmonic effect of metallic nanostructures [12]. The fundamental interactions between surface plasmons and fluorescent molecules had gained a great interest from researchers to improve the physical insight

* Corresponding author. Department of Physics & Astronomy, Science College, King Saud University, Riyadh, Saudi Arabia. Tel.: +966 565850487; fax: +966 14673656.

E-mail address: elbashireg@yahoo.com (S.M. El-Bashir).

on the design rules for metallic nanoparticles tailored to plasmonic thin film luminescent solar concentrators PTLSC applications [13–15].

The main objective of the proposed work is to enhance the power conversion efficiency of bilayer PTLSCs shown in Fig. 1, by increasing the interplay phenomena between fluorescence and localized surface Plasmon resonances of MNPs. PTLSC waveguides were prepared by coating polycarbonate (PC, $n = 1.586$) substrates by two layers, the bottom layer consists of 50 μm fluorescent polymethylmethacrylate (PMMA) film doped with mixed coumarin dyestuffs, silver and gold nanoparticles (AgNPs, AuNPs). The top layer consists of 20 μm PMMA/0.5wt%SiO₂ nanohybrid which acts as a highly refractive index coating ($n = 1.585$) [2]. This configuration provides a broadband enhancement of light harvesting by the luminescent centers in the primary layer which is sandwiched between two high index regions due to: (1) the increase of the effective absorption cross-section of luminescent centers leading to a nearly full-spectrum absorption of solar photons, (2) enhancement spontaneous emission by surface plasmons and Purcell effect, and (3) improvement of the quantum efficiency of luminescent centers [16].

2. Experimental

2.1. Materials

Polymethylmethacrylate (PMMA, 350k) was obtained from Aldrich, USA. Coumarin dyestuffs MACROLEX Fluorescent Red G and MACROLEX Fluorescent Yellow 10 GN were obtained from Bayer, Germany. Spherical AgNPs and AuNPs with average particle diameters 60 and 100 nm were obtained from Aldrich (USA). HPLC grade Dichloromethane (CH₂Cl₂) was obtained from Aldrich (USA) and used as high purity solvent for PMMA grains. Transparent Polycarbonate (PC) sheets of 3 mm thickness were obtained from Rohm (Germany).

2.2. Preparation of PTLSC films

PTLSC films were prepared from metal enhanced fluorescent PMMA films by adding AuNPs with different concentrations ranging from 5 to 25 ppm to PMMA/CH₂Cl₂ solution containing (70 ppm MACROLEX Fluorescent Yellow 10 GN, 30 ppm MACROLEX Fluorescent Red G, and 20 ppm AgNPs respectively). All the polymer solutions were sonicated for 6 h before pouring on glass

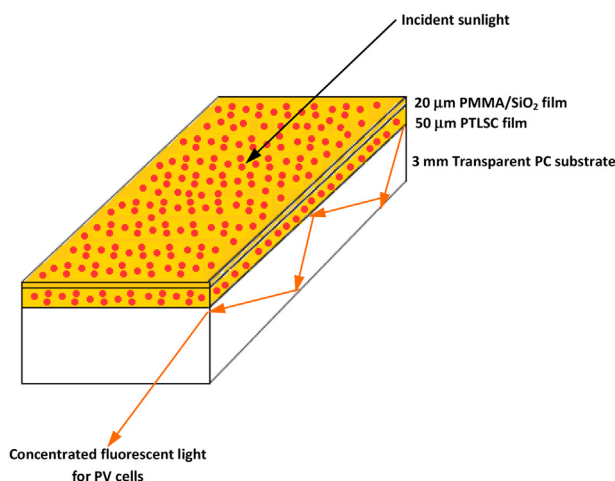


Fig. 1. Plasmonic thin film luminescent solar concentrator (PTLSC).

substrates and spin coated in a centrifuge at 2000 rpm for 1 min to obtain uniform film coverage [3,8], then they are left to dry in an electric oven at 40 °C for 6 h. The film thicknesses were measured using a profilometer (Talystep, Taylor Hobson, UK) on a scratch made immediately after deposition of five independent measurements on each sample, and found to be in the range of $50 \pm 10 \mu\text{m}$ [17]. Fluorescence spectroscopy measurements revealed that PTLSC films are promising candidates for preparing efficient waveguides and for harvesting and concentrating sunlight as presented by the subject of another paper submitted by our group [18].

2.3. Preparation of PTLSC waveguides

Using the same procedure described before; bilayer PTLSC waveguides were prepared by spin coating of PMMA/CH₂Cl₂ solution (prepared as described in the previous section) on PC rectangular plates with dimensions of $(20 \times 8 \times 0.3 \text{ cm}^3)$, the thickness of this optically active layer was 50 μm . After that PC plates were coated with a second 20 μm layer of PMMA/SiO₂ nanohybrid which is very important to increase the light-pipe trapping, scratch resistant thermal and photostability of fluorescent molecules [2,3]. After each coating process the plates were left to be dry firstly at room temperature and then in an electrical furnace at 50 °C for 3 h. Fig. 2 illustrates the photographs of PTLSCs waveguides doped with different AuNPs concentrations.

2.4. Characterization and measurements

The absorption spectra were recorded in the wavelength range (190–900 nm) using a UV–vis spectrophotometer (UNICAM, Helios Co., Germany). The steady-state fluorescence spectra were recorded in the wavelength range (400–800 nm) using a spectrofluorimeter (Perkin Elmer LS 50 B, UK). The effect of AuNPs concentration on the photoresponse of the prepared PTLSC films toward simulated sunlight was performed using a Xenon-arc lamp with the aid of the photodegradation accelerator (SUNTEST XLS+, Germany). The films were irradiated by $1200 \text{ kJ m}^{-2} \text{ h}^{-1}$ continuously for 24 h to eliminate the dark reactions which might occur under normal day–night cycles. This period is equivalent to the global solar irradiance for about one year exposure to natural sunlight and the apparatus was regulated to match the climatic conditions of Riyadh city (KSA).

2.5. I–V characteristics of PTLSCs

PTLSCs prototypes were tested indoors by being illuminated by AM1.5 artificial solar spectrum with the aid of 300 W solar

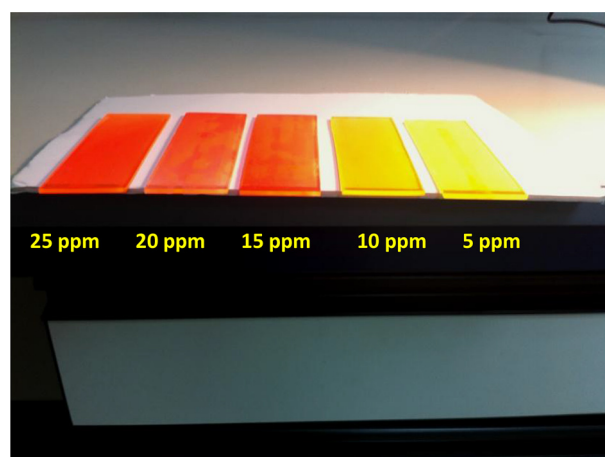


Fig. 2. PTLSCs waveguides containing different AuNPs concentrations.

simulator (Lot-Oriel, Germany). In order to identify the conversion power efficiency enhancement, three types of silicon PV cells were attached to one narrow edge of each PTLSC shown in Fig. 2, while the other edges were painted with a high quality diffused reflectance paint ($\sim 98\%$ Kodak, Japan). Commercial silicon PV cells were used: single crystalline (c-Si), multicrystalline (mc-Si) and amorphous (a-Si), all obtained from (SILICON SOLAR Co., USA). The I – V characteristics were measured for all PV cells before and after being attached to PTLSCs using a digital multimeter (PeakTech, Germany).

2.6. Outdoor testing of PTLSCs

The hourly outdoor testing of a prototype PTLSC was done for six months under clear sky conditions during winter and spring seasons considering the day 21 as the reference day for each month. The global solar radiation was measured hourly along with the PTLSC testing at Riyadh city (37° N) on the roof of a building about 10 m height using an accurate solar power meter (SPM-1116 SD., Taiwan). For accurate detection for the light collected by PTLSC we selected c-Si PV cells to be attached to PTLSC waveguide having 10 ppm AuNPs concentration.

The output short circuit current of the PV cell (I_{PTLSC}) attached to PTLSC was measured hourly along with that of the reference PV cell (I_{ref}) exposed directly to sunlight in order to calculate the optical efficiency (η_{opt}).

3. Results and discussion

3.1. Light harvesting and energy transfer of PTLSC films

Fig. 3 shows the absorption spectra of MACROLEX fluorescent dyes, AgNPs and AuNPs in cases of being doped individually and altogether in PMMA films. The absorption spectrum for each of these dopants is characterized by a single broad peak, the individual absorption maxima were found at 450, 460, 522 and 570 nm for Yellow GN, AgNPs, Red G and AuNPs respectively. It is clear that AgNPs have their maximum absorption at 460 nm in PMMA which represents the wavelength having the lowest percentage of the visible solar spectrum since it has the highest intensity at about 550 nm [2]. Therefore in order to enhance the absorption of PTLSCs we intended to use AuNPs besides AgNPs due to their extended absorption in the visible region, recommending a potential light harvesting of the visible solar spectra. On the other hand, the profile

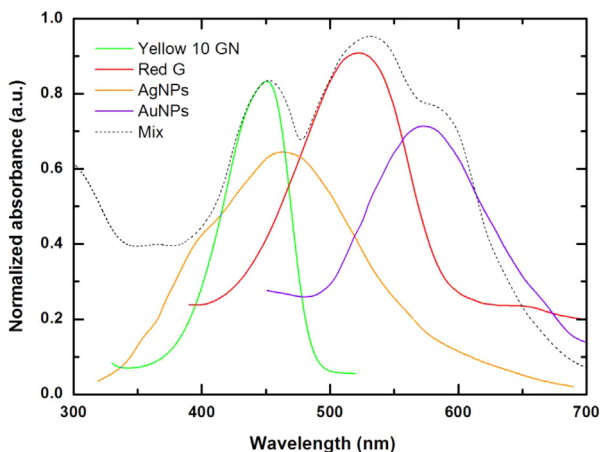


Fig. 3. Absorption spectra of MACROLEX Fluorescent dyes and noble metal nanoparticles doped in PMMA individually and as a mixture.

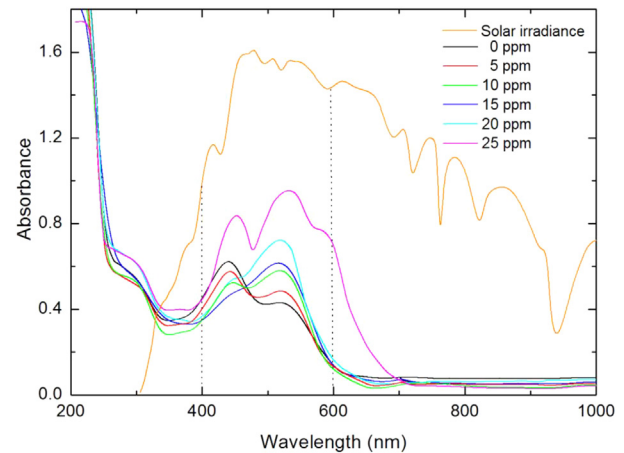


Fig. 4. Effect of AuNPs concentration on the absorption spectra of PTLSC films compared to normalized AM1.5 solar spectrum.

of the absorption spectra of the combined dopants is dependent on the shape of the individual spectrum of each dopant [7] and found to extend from 400 to 600 nm with a maximum optical density 0.95 originated at 530 nm. Following this rationale we incorporated AuNPs to PTLSC films to enhance the light absorption and fluorescence intensity [19]. Figs. 4 and 5 show the absorption and fluorescence spectra of the prepared PTLSC films depicted together with the solar spectrum at AM1.5, from this illustration it can be clarified that the visible solar spectra are approximately covered by the absorption and MEF spectra of PTLSCs.

The spectral sensitivity of commercial silicon PV cells is shown in Fig. 6 and plotted along with normalized fluorescence spectra of PTLSC films. In fact the spectral sensitivity of silicon is influenced by its production method [20], it is observed that the sensitivity ranges for silicon PV cells are from 500 to 1125 nm for c-Si, from 375 to 1100 nm for mc-Si and from 410 to 775 nm for a-Si. It is noted that the maximum overlap had occurred between the spectral response of c-Si, mc-Si and a-Si PV cells and the fluorescence maxima of PTLSC films doped with 10, 25, 20 ppm AuNPs. This standing for the applicability of the prepared PTLSC films to overcome the poor performance of silicon PV cells at short wavelengths since their fluorescence maxima could be detected all the types silicon PV cells [21].

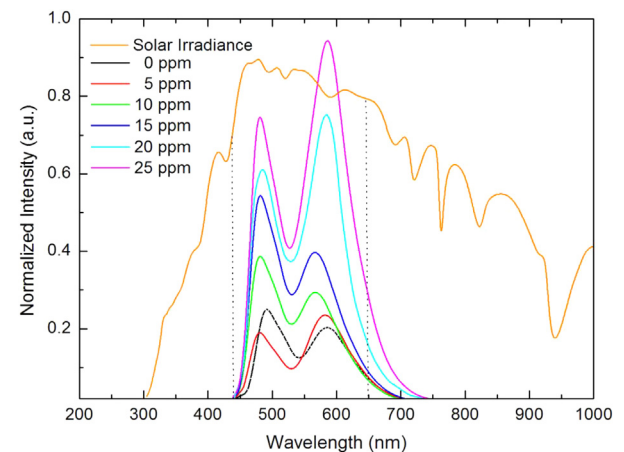


Fig. 5. Metal enhanced fluorescence of PTLSC films at different AuNPs concentrations (the data is normalized with AM1.5 solar spectrum).

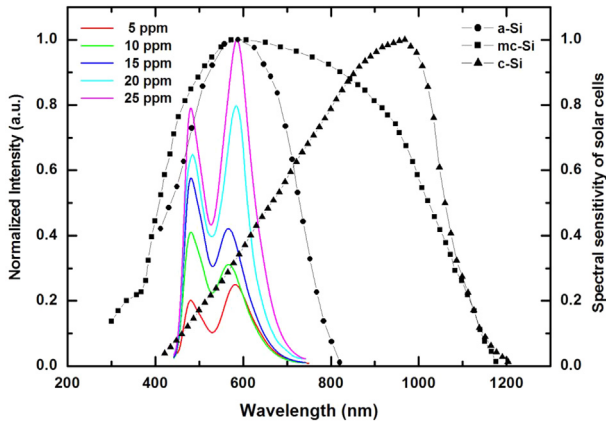


Fig. 6. Spectral response of silicon PV cells compared to the fluorescence spectra of PTLSCs.

3.2. Interband HOMO–LUMO transitions in PTLSC films

The absorption edges of the prepared PTLSC films were analyzed in order to know the electronic transitions from the highest occupied molecular orbital(s) (HOMO) of the valence band to the lowest unoccupied molecular orbital(s) of the conduction band (LUMO) which are directly related to the matrix stability [22]. The fundamental absorption coefficient “ α ” of photon energy “ E ” is related to interband transitions according to the type of transition through the band gap [23], the usual method to determine the energy of the band gap is to plot a graph between $(\alpha E)^{1/m}$ versus “ E ” looking for the value of “ m ” depending on the nature of transition. The allowed direct and indirect interband transitions are given by the values of “ m ” as $1/2$ and 2 respectively [21]:

$$\alpha E = A(E - E_{gd})^{1/2} \quad (1)$$

$$\alpha E = B \left[\frac{(E - E_{gi} + E_p)^2}{\exp(E_p/kT) - 1} + \frac{(E - E_{gi} - E_p)^2}{1 - \exp(-E_p/kT)} \right] \quad (2)$$

where A and B are constants, k is Boltzmann constant, T is the absolute temperature, E_p is the phonon energy, E_{gd} and E_{gi} are the

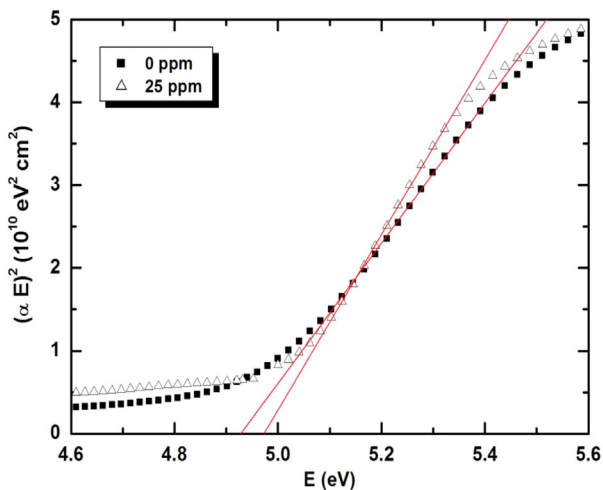


Fig. 7. Effect of AuNPs concentration on the direct gap interband transitions, E_{gd} , in PTLSC films.

Table 1

Effect of AuNPs concentration on the direct and indirect HOMO–LUMO interband transitions for PLSC films.

Concentration (ppm)	E_g (eV)	E_{gi} (eV)
0	4.92	3.80
5	4.94	3.84
10	4.93	3.83
15	4.86	3.82
20	4.87	3.81
25	4.97	3.82

energies of direct and indirect interband transitions respectively [21]. According to equations (1) and (2), there will be a single straight line for direct transitions and two linear portions for indirect transitions. Equations (1) and (2) were applied for all the PTLSC films and the relation between $(\alpha E)^2$ against “ E ” is plotted in Fig. 7. The values of direct interband transition, E_{gd} , were estimated from the intercept on the energy axis of the linear fit of the large energy data of the plot and listed in Table 1.

Fig. 8 shows that plotting $(\alpha E)^{1/2}$ against “ E ” that resolved into two distinct straight-line portions, the straight line obtained at lower photon energies, corresponding to phonon-absorption process, cuts the energy axis at $E_{gi} - E_p$. The other line represents the dependence in the high energy range corresponding to a phonon-emission process and cuts the energy axis at $E_{gi} + E_p$, from the energy intercept of the two straight line portions, the values of the indirect HOMO–LUMO transition E_{gi} could be estimated and listed in Table 1. It is noted that the values of both transitions appeared around one value as $E_{gd} \sim 4.9$ eV and $E_{gi} \sim 3.8$ eV, this behavior is in a good agreement with the attained MEF in Fig. 4 since there is considerable spectral shift in the fluorescence maxima. The larger values of E_{gd} can be attributed to the fact that AuNPs introduced localized levels that form a continuum which act as trapping states and consequently increase E_{gd} [22]. In addition the indirect interband transition energy E_{gi} which can be attributed to the existence different types of excitons [24], which is found to be well correlated behavior to the absorbance spectra shown in Fig. 4 since it showed more than one maximum. The steadiness of the interband transition energies indicates the advantage of AuNPs in reducing the probability of the dye interaction with the defects of PMMA and consequently the stability of the HOMO–LUMO interband transitions of PTLSCs [25].

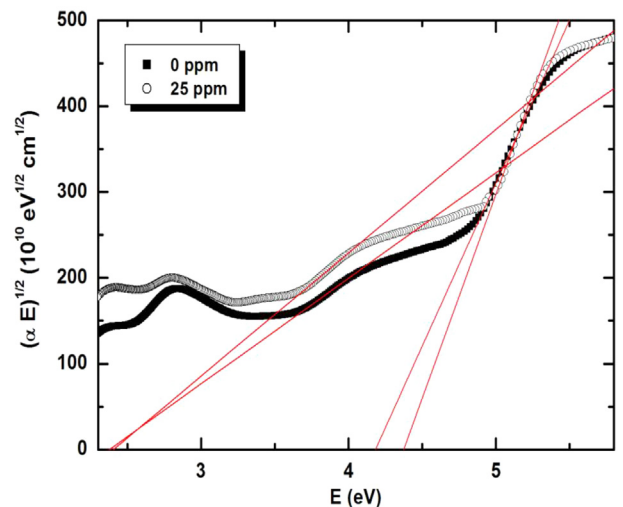


Fig. 8. Effect of AuNPs concentration on the indirect gap interband transitions, E_{gi} , in PTLSC films.

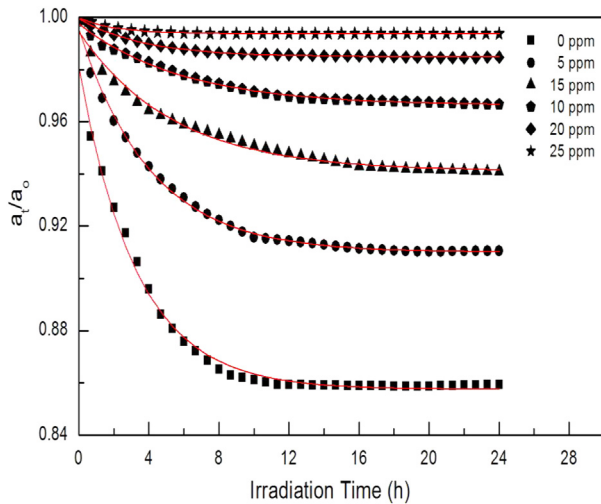


Fig. 9. Effect of AuNPs concentration on the photodegradation curves of PTLSC films, after indoor exposure to artificial sunlight from a Xenon arc lamp.

3.3. Indoor photostability test of PTLSC films

Testing under the conditions that approximate the intended service environment requires months or years to obtain results; hence test conditions that greatly accelerate the degradation had to be used [26]. The percentage change in the absorption maxima of the mixed dyes was monitored at different times during the irradiation period. The photodegradation a_t/a_0 , which is the percentage change of optical density after irradiation is plotted versus the exposure time as illustrated in Fig. 9. It was found that the behavior obeys the exponential relation described by the 1st order exponential decay function [26],

$$a_t/a_0 = C_1 \exp(-Rt) + C_2 \quad (3)$$

where C_1 is a constant, R is the photodegradation rate constant of dye molecules and C_2 represents the percentage change of the absorption after the irradiation period. The Photodegradation of dye molecules occurs by two mechanisms [26], the first concerns the dye molecules which may exist outside the core, and takes a short time to photodecompose; the second mechanism concerns the photodecomposition of the caged dye molecules inside the free volume of crosslinked PMMA chains, the values of R and C_2 were calculated and listed in Table 2. It is obviously noted that the photodegradation rate of the investigated dye mixture is decreased to about 15.5% about of its initial value after the incorporation of 25 ppm AuNPs which acts as metallic nano-pigment [27]. Another advantage was achieved by observing the values of C_2 , the dye absorbance reaches about 99% of its initial value after adding 25 ppm AuNPs which is the period corresponding to the stability of this matrix to one year exposure to natural sunlight in Riyadh city.

Table 2
Effect of AuNPs concentration on the photodegradation parameters of PLSC films.

Concentration (ppm)	R (s^{-1})	C_2 %
0	8.40×10^{-5}	86
5	6.83×10^{-5}	91
10	5.15×10^{-5}	94
15	4.73×10^{-5}	97
20	2.39×10^{-5}	98
25	1.30×10^{-5}	99

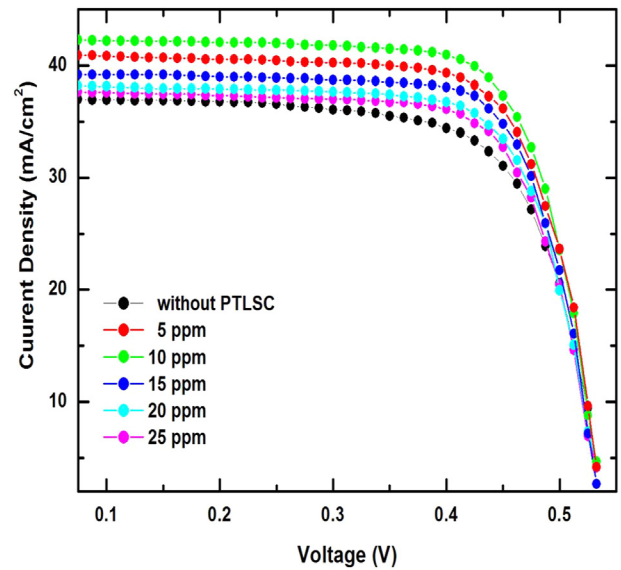


Fig. 10. Photovoltaic output of c-Si PV cell before and after being attached to PTLSCs.

3.4. Indoor testing of PTLSC waveguides

Figs. 10–12 show typical I – V characteristics for c-Si, mc-Si and a-Si PV cells before and after being attached to PTLSCs. It is clear that the photovoltaic output is strongly dependent on the concentration of gold nanoparticles of each plate. The increase of photovoltaic output of each cell was determined by monitoring the change in the I – V curve for silicon PV cells before and after being attached to PTLSCs.

Table 3 shows the percentage change of short-circuit current for all the PV cells after and before being attached to PTLSCs (I_{PTLSC}/I_{PV}). It is observed that the maximum values of I_{sc} enhancement were 50%, 38% and 14% obtained for a-Si and mc-Si and c-Si PV cells respectively. The considerable enhancement for a-Si and mc-Si solar cells can be ascribed to the coincidence of their spectral response at the fluorescence wavelength of PTLSCs doped with 20 and 25 ppm AuNPs [22], as previously mentioned in Fig. 6. On the other hand the poor enhancement in c-Si PV cell can be attributed

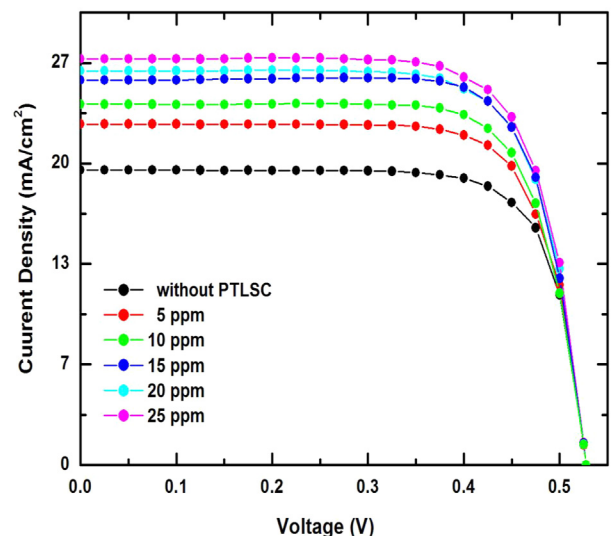


Fig. 11. Photovoltaic output of mc-Si PV cell before and after being attached to PTLSCs.

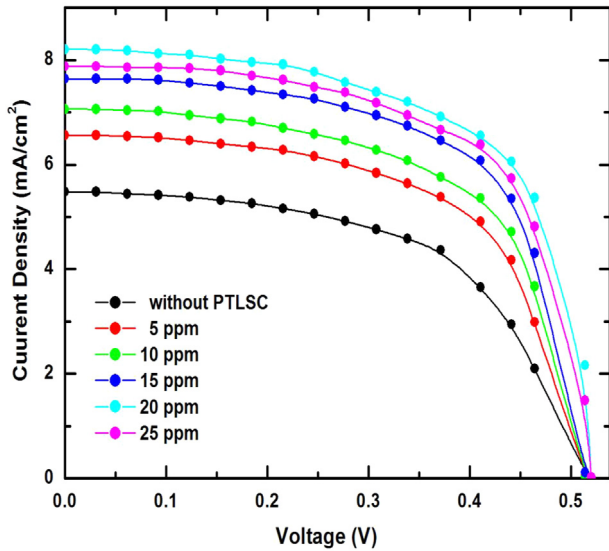


Fig. 12. Photovoltaic output of a-Si PV cell before and after being attached to PTLSCs.

to the fact that a relatively low-energy gap (1.3 eV) which leads to low photon harvesting in the visible regions [21].

The power conversion efficiency (η) of PV cells which is the percentage of power converted from absorbed light to electrical energy, can be calculated as the ratio of maximum output power (P_{out}) divided by the input light power (P_{in}) under standard test conditions [28]. The enhancement in the conversion power efficiency ($\Delta\eta\%$) can be calculated as follows,

$$\Delta\eta\% = [(\eta_{PTLSC\%} - \eta_{PV\%}) / \eta_{PV\%}] \times 100 \quad (4)$$

where $\eta_{PTLSC\%}$ is the power conversion of the PV cell attached to PTLSCs and $\eta_{PV\%}$ is the efficiency of PV cell.

Table 4 shows the values of $\Delta\eta\%$ for silicon PV cells attached to PTLSCs which reached the maximum values 53.24, 33.4 and 25.8% for a-Si, mc-Si and c-Si PV cells attached to PTLSCs doped with 25, 20 and 10 ppm AuNPs. This enhancement can be ascribed to the efficient energy transfer through the photon harvesting antenna PTLSC systems that spectrally convert, concentrate and guide the light toward the active layer of PV cells by metal enhanced fluorescence. The energy transfer processes presented here are expected to overcome the problem of incomplete absorption of solar spectra specially for low-efficiency solar cells [7]. To achieve the

Table 3
The effect of AuNPs concentration on the ratio (I_{PTLSC}/I_{PV}) for PTLSCs.

PV cell	5 ppm	10 ppm	15 ppm	20 ppm	25 ppm
a-Si	1.20	1.30	1.40	1.50	1.44
mc-Si	1.16	1.22	1.31	1.34	1.40
c-Si	1.10	1.14	1.06	1.03	1.02

Table 4
The effect of AuNPs concentration on the efficiency enhancement ($\Delta\eta\%$) of silicon PV cells attached to PTLSCs.

PV cell	a-Si	mc-Si	c-Si
5 ppm	25.63	26.07	15.14
10 ppm	35.70	26.79	25.80
15 ppm	44.27	30.51	12.00
20 ppm	53.20	31.78	7.30
25 ppm	51.56	33.40	5.54

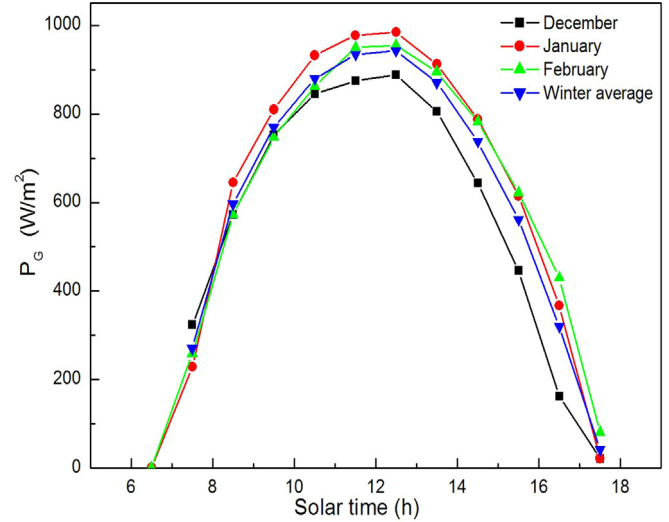


Fig. 13. The hourly distribution of the global solar energy radiation in Riyadh (winter 2012).

largest possible enhancement, one must create a structure where the luminescent species are located in the range of optimum enhanced localized electromagnetic field of the metal nanoparticles. This study is of great importance of the effective concentration ratio of PTLSCs given that the localized SPR phenomenon of AuNPs is responsible for both increased absorption and excitation rate of fluorescent dyes in PTLSC films [11].

3.5. Outdoor performance of PTLSC waveguides

Firstly, we measured the daily global solar radiation falling on a horizontal surface, P_g , was measured hourly for winter and spring seasons at Riyadh city (KSA-2012), and plotted as shown in Figs. 13 and 14. It is noticed that the global solar radiation curves versus the time of the day reaches its maximum value at the solar noon of each month. The maximum value of P_g was 1040 W/m² recorded in May, so it is greatly revealed that Riyadh city is one of the world's most productive solar regions and qualified as a potential candidate for solar energy utilization. In addition the observed decrease of the seasonal average values of P_g was attributed to the vagaries of the weather and the spread of clouds in winter months and dust in

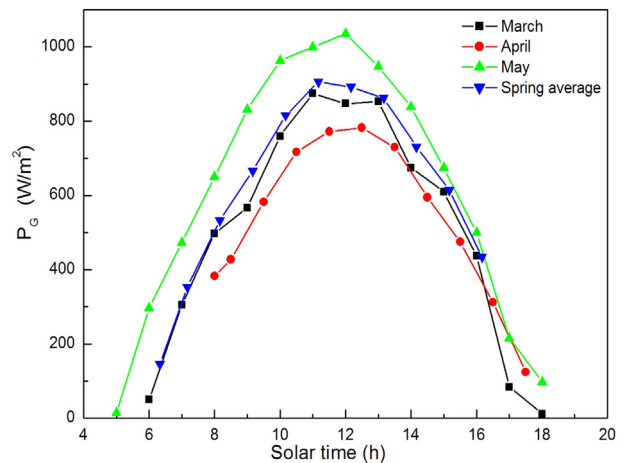


Fig. 14. The hourly distribution of the global solar energy radiation in Riyadh (spring 2012).

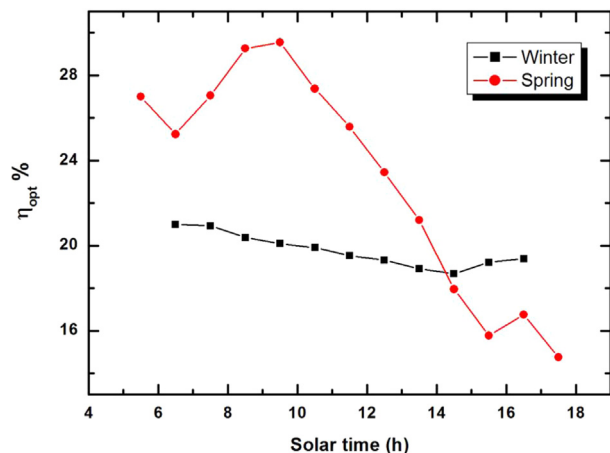


Fig. 15. The hourly distribution of the optical efficiency, η_{opt} , for winter and spring seasons (Riyadh-2012).

March and April months. From these plots one can be provided by useful information about, the sunrise time, the sunset time, the peak power at solar noon and subsequently determining the day length on the basis of which the outcome of a solar conversion system can be evaluated [29].

The outdoor testing of the optical efficiency, η_{opt} , was performed for horizontally mounted PTLSC plate doped with 10 ppm AuNPs, the values of η_{opt} were calculated hourly under day light illumination for winter and spring seasons at Riyadh city (KSA-2012) using the following equation [26]

$$\eta_{opt} = \left(I_{sc}/I_{ref} \right) (B/G) \quad (5)$$

where I_{PTLSC} and I_{ref} are the short circuit current values of the PV cells attached to PTLSC edge and the reference PV cells directly exposed to sunlight respectively, G is the geometric gain defined as the ratio of the surface area to the edge area of the PTLSC plate and B is the ratio of PV cell response at the fluorescence wavelength to the corresponding response of solar spectra.

Fig. 15 demonstrates a plot of the hourly values of η_{opt} for the investigated PTLSC averaged over the winter and spring seasons, besides the monthly average values of η_{opt} listed in Table 5. For winter season, it is clear that, the hourly average values of η_{opt} increase at the sunrise and sunset and decrease around the midday in well agreement with our published work [26]. This behavior can be ascribed due to the decrease of the direct light component near the time of sunrise and sunset besides the overcast weather caused by cloudy sky at this time of year (winter 2012). From the practical point of view it is advantageous since the PTLSCs have a high efficiency under both clear and cloudy sky conditions [30]. On the other hand, this behavior observed is inverted in spring, which can be explained by the fact that most of solar radiation in Riyadh is direct according to its high altitude angle, in view of the fact that the global solar radiation falling on a horizontal surface is given by [31]

Table 5
The seasonal average values of η_{opt} %.

Winter		Spring	
December	19.70	March	20.80
October	19.30	April	19.50
November	20.20	May	28.00
Average	19.70	Average	23.15

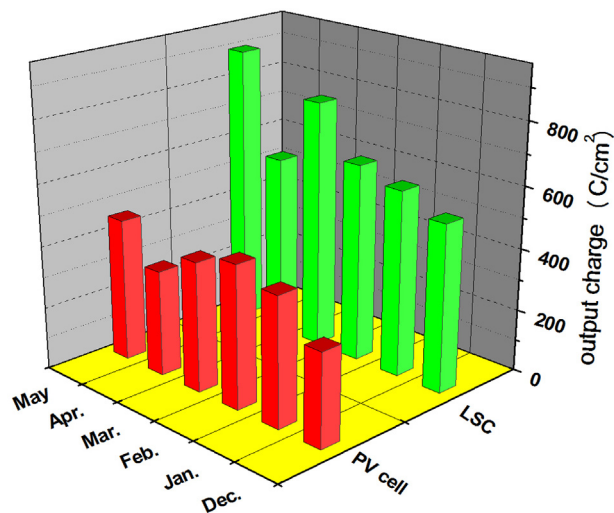


Fig. 16. The area under the J_{sc} -solar time curves plotted in comparison with that of a reference PV cell for all months.

$$P_G = P_D + P_B \sin \gamma \quad (6)$$

where P_D is the diffused solar radiation, P_B is the direct (beam) component and γ is the solar altitude angle of the location. The decrease of the spring average value of η_{opt} near the sunset and sunrise can be attributed to low amount of diffused radiation as a result of the high clearness index K_T in Riyadh [32] at most of the year months according to the following equation [33,34]

$$P_D/P_G = 1 - 1.13K_T \quad (7)$$

Table 5 shows that the maximum average value of η_{opt} is obtained for May month (28%) due to the augmented global solar irradiance in this month as a result of the increase of direct component in the vicinity to the beginning of summer [35].

The area under the current density curve (J_{sc}) versus solar time was calculated and plotted in comparison with that of a reference PV cell for the months concerned in our study as shown in Fig. 16. It is observed that the maximum solar electrical conversion was obtained for May, these results showed a well correlation between the solar energy conversion and the solar power input of each month [26].

4. Conclusion

Bilayer PTLSC waveguides were prepared by spin coating of fluorescent PMMA nanohybrid solution on PC substrates. Indoor photostability measurements showed a remarkable decrease in the photodegradation rate of coumarin dyestuffs by increasing the concentration of AuNPs which acts as a metallic nano-pigment providing long lifetime PTLSCs. Another advantage of AuNPs is the role of reducing the probability of the dye interaction with the film defects which resulted in the observed steadiness in the photophysical processes occurred in the HOMO–LUMO interband transitions of the optically active layer of PTLSCs. Laboratory studies of the I – V characteristics of silicon PV cells attached to PTLSCs proved a promising approach to improve solar energy harvesting since the enhancement in the short circuit current values was 50%, 38% and 14% obtained for a-Si, mc-Si and c-Si PV cells respectively.

The outdoor testing of PTLSC prototype revealed that the best light concentration be attained by using a spectrally adapted PV cell specially in overcast weather. Finally, it is concluded that the

development of plasmonic structures had opened the feasibilities for plasmonic applications in the field of solar energy conversion.

Acknowledgment

This research project was supported by a grant from the “Research Center of the Female Scientific and Medical Colleges”, Deanship of Scientific Research, King Saud University.

References

- [1] Goodall C. Ten technologies to fix energy and climate. Profile books. 2nd ed.; July 21, 2012. ISBN-10: 3847306855 ISBN-13: 978-3847306856.
- [2] El-Bashir SM. Photophysical properties of PMMA nanohybrids and their applications: luminescent solar concentrators & smart greenhouses. LAMPERT Academic Publishing; 2012. ISBN 978-38473-0685-6; 2012.
- [3] El-Bashir SM. Photophysical properties of fluorescent PMMA/SiO₂ nanohybrids for solar energy applications. *J Lumin* 2012;132:1786–91.
- [4] van Sark WG, Barnham KW, Slooff LH, Chatten AJ, Büchtemann A, Meyer A, et al. Luminescent solar concentrators – a review of recent results. *Opt Express* 2008;16:21773–92.
- [5] Rowan BC, Wilson LR, Richards BS. Advanced material concepts for luminescent solar concentrators. *IEEE J Select Top Quant Electron* 2008;14:1312–22.
- [6] Debije Michael G, Verbunt Paul PC. Thirty years of luminescent solar concentrator research: solar energy for the built environment. *Adv Energy Mater* 2012;2:12–35.
- [7] Bailey ST, Lokey GE, Hanes MS, Shearer JDM, McLafferty JB, Beaumont GT, et al. Optimized excitation energy transfer in a three-dye luminescent solar concentrator. *Sol Energy Mater Sol Cells* 2007;91:67–75.
- [8] Reisfeld R, Shamrakov D, Jorgensen C. Photostable solar concentrators based on fluorescent glass-films. *Sol Energy Mater Sol Cells* 1994;33:417–27.
- [9] Hughes MD, Maher C, Tasciuc DAB, Polanco D, Kaminski D. Performance comparison of wedge-shaped and planar luminescent solar concentrators. *Renew Energy* 2013;52:266–72.
- [10] Buffa M, Carturan S, Debije MG, Quaranta A, Maggioni G. Dye-doped polysiloxane rubbers for luminescent solar concentrator systems. *Sol Energy Mater Sol Cells* 2012;103:114–8.
- [11] Chandra S, Doran J, McCormack SJ, Kennedy M, Chatten AJ. Enhanced quantum dot emission for luminescent solar concentrators using plasmonic interaction. *Sol Energy Mater Sol Cells* 2012;98:385–90.
- [12] Yang J, You J, Chen CC, Hsu WC, Tan HR, Zhang XW, et al. Plasmonic polymer tandem solar cell. *ACS Nano* 2011;5:6210–7.
- [13] Asim N, Sopian K, Ahmadi S, Saeedfar K, Alghoul MA, Saadatian O, et al. A review on the role of materials science in solar cells. *Renew Sustain Energy Rev* 2012;16:5834–47.
- [14] Levchenko V, Grouchko M, Magdassi S, Saraidarov T, Reisfeld R. Enhancement of luminescence of Rhodamine B by gold nanoparticles in thin films on glass for active optical materials applications. *Opt Mater* 2011;34:360–4.
- [15] Reisfeld R, Pietraszkiewicz M, Saraidarov T, Levchenko V. Luminescence intensification of lanthanide complexes by silver nanoparticles incorporated in sol–gel matrix. *J Rare Earths* 2009;27:544–9.
- [16] Xiao Y-F, Zou C-L, Hu Y-W, Li Y, Xiao L, Sun F-W, et al. Broadband enhancement of light harvesting in a luminescent solar concentrator. *IEEE J Quant Electron* 2011;47:1171–6.
- [17] Pepe A, Galliano P, Aparicio M, Duran A, Cere S. Sol–gel coatings on carbon steel: electrochemical evaluation. *Surf Coat Technol* 2006;200:3486–91.
- [18] El-Bashir SM, Barakat FM, AlSalhi MS. Plasmon enhanced fluorescence of mixed coumarin dyes by noble metal nanoparticles: towards plasmonic thin film luminescent solar concentrator. *J Lumin* 2013;143:43–9.
- [19] Lakowicz JR. Radiative decay engineering 5: metal-enhanced fluorescence and plasmon emission. *Anal Biochem* 2005;337:171–94.
- [20] Neuroth N, Haspel R. Glasses for luminescent solar concentrators. *Sol Energy Mater Sol Cells* 1987;16:235–42.
- [21] Ahmed RM, El-Bashir SM. Structure and physical properties of polymer composite films doped with fullerene nanoparticles. *Int J Photoenergy* 2011;2011. Article ID 801409.
- [22] Mansour AF, El-Shaarawy MG, El-Bashir SM, El-Mansy MK, Hammam M. Optical study of perylene dye doped poly(methyl methacrylate) as fluorescent solar collector. *Polym Int* 2002;51:393–7.
- [23] Fox M. Optical properties of solids. New York: Oxford University Press Inc.; 2001.
- [24] Kulyk B, Kapustianyk V, Tsybul'skyy V, Krupka V, Sahraoui O. Optical properties of ZnO/PMMA nanocomposite films. *J Alloys Compd* 2010;502:24–7.
- [25] Švorcik V, Lyutakov O, Huttel I. Thickness dependence of refractive index and optical gap of PMMA layers prepared under electrical field. *J Mater Sci: Mater Electron* 2008;19:363–7.
- [26] El-Shaarawy MG, El-Bashir SM, Hammam M, El-Mansy MK. Bent fluorescent solar concentrators (BFSCs): spectroscopy, stability and outdoor performance. *Curr Appl Phys* 2007;7:643–9.
- [27] Blosi M, Albonetti S, Gatti F, Baldi G, Dondi M. Au–Ag nanoparticles as red pigment in ceramic inks for digital decoration. *Dyes Pigm* 2012;94:355–62.
- [28] Nelson J. The physics of solar cells. Imperial College Press; 2003. ISBN 978-1-86094-340-9; 2003.
- [29] Badescu V. Modeling solar radiation at the earth's surface: recent advances. ISBN 978-3540774549; 2008.
- [30] Mansour AF, El-Shaarawy MG, El-Bashir SM, El-Mansy MK, Hammam M. A qualitative study and field performance for a fluorescent solar collector. *Polym Test* 2002;21:277–81.
- [31] Iqbal M. An introduction to solar radiation. New York: Academic Press; 1983.
- [32] Sahin AZ, Aksakal A, Kahraman R. Solar radiation availability in the north-eastern region of Saudi Arabia. *Energy Sources* 2000;22:859–64.
- [33] Ulgen K. Optimum tilt angle for solar collectors. *Energy Sources* 2006;28:1171–80.
- [34] Falayi EO, Rabiou AB, Teliat RO. Correlations to estimate monthly mean of daily diffuse solar radiation in some selected cities in Nigeria. *Adv Appl Sci Res* 2011;2:480–90.
- [35] Aljarboua Z. The national energy strategy for Saudi Arabia world academy of science. *Eng Technol* 2009;33:501–10.